Astronomy & Astrophysics

LETTER TO THE EDITOR

Refinement of the convex shape model and tumbling spin state of (99942) Apophis using the 2020–2021 apparition data

H.-J. Lee[1], M.-J. Kim[1], A. Marciniak[2], D.-H. Kim[1,3], H.-K. Moon[1], Y.-J. Choi[1,4], S. Zoła[5], J. Chatelain[7],
T. A. Lister[7], E. Gomez[8], S. Greenstreet[9,10], A. Pál[11], R. Szakáts[11], N. Erasmus[12], R. Lees[13],
P. Janse van Rensburg[12,13], W. Ogłoza[6], M. Dróżdż[6], M. Żejmo[14], K. Kamiński[2], M. K. Kamińska[2], R. Duffard[15],
D.-G. Roh[1], H.-S. Yim[1], T. Kim[16], S. Mottola[17], F. Yoshida[18,19], D. E. Reichart[20], E. Sonbas[21,25], D. B. Caton[22],
M. Kaplan[23], O. Erece[23,24], and H. Yang[1]

(Affiliations can be found after the references)

ABSTRACT

Context. The close approach of the near-Earth asteroid (99942) Apophis to Earth in 2029 will provide a unique opportunity to examine how the physical properties of the asteroid could be changed due to the Earth's gravitational perturbation. As a result, the Republic of Korea is planning a rendezvous mission to Apophis.
Aims. Our aim was to use photometric data from the apparitions in 2020−2021 to refine the shape model and spin state of Apophis.
Methods. Using thirty-six 1- to 2-meter-class ground-based telescopes and the Transiting Exoplanet Survey Satellite, we carried out a photometric observation campaign throughout the 2020−2021 apparition. The convex shape model and spin state were refined using the light-curve inversion method.
Results. According to our best-fit model, Apophis is rotating in a short-axis mode with rotation and precession periods of 264.178 h and 27.38547 h, respectively. The angular momentum vector orientation of Apophis was found to be (275°, −85°) in the ecliptic coordinate system. The ratio of the dynamic moments of inertia of this asteroid was fitted to $I_a:I_b:I_c = 0.64:0.97:1$, which corresponds to an elongated prolate ellipsoid. These findings regarding the spin state and shape model can be used to both design the space mission scenario and investigate the impact of the Earth's tidal force during close encounters.

Key words. minor planets, asteroids: individual: (99942) Apophis – techniques: photometric

1. Introduction

The Aten-type near-Earth asteroid (99942) Apophis (2004 MN4, hereafter Apophis) is an Sq-type asteroid with an estimated size of 340 m (Binzel et al. 2009; Brozović et al. 2018; Reddy et al. 2018). It was discovered on June 19, 2004, by R. A. Tucker, D. J. Tholen, and F. Bernardi at Kitt Peak, Arizona. From early predictions, it was estimated that this asteroid could impact Earth with a maximum probability of 2.7% (Jet Propulsion Laboratory Sentry on December 27, 2004; Chesley 2006). As the accuracy of the orbital prediction improved in follow-up observations, the impact probability of Apophis was reduced. In particular, the prediction derived from high-precision radar observations at the Arecibo Observatory in 2005 and 2006 indicated that it would pass by Earth in April 2029 at a geocentric distance of 38 326 km (approximately six Earth radii), which is within the geosynchronous orbit in April 2029 (Giorgini et al. 2008). Recently, radar observations made in March 2021 at the Goldstone Solar System Radar and the Green Bank Telescope were used to precisely estimate Apophis's orbit around the Sun, ruling out any Earth impact threat for the next hundred years or more (Greicius 2021).

Although Apophis's impact threat has disappeared, this asteroid remains an object of interest because of its close approach in 2029. The 2029 Earth encounter is expected to trigger varying degrees of alterations in the dynamics, spin states, and surface arrangements of Apophis due to the Earth's gravitational perturbation (Yu et al. 2014; Souchay et al. 2014, 2018; DeMartini et al. 2019; Hirabayashi et al. 2021; Valvano et al. 2022). Thus, the study of this asteroid will provide an excellent opportunity to examine the evolutionary process of its physical properties caused by planetary perturbation. For this reason, Apophis became a unique observation target and is the primary mission target of the Rendezvous Mission to Apophis, which is currently under pre-phase A study in the Republic of Korea and is scheduled for launch in 2027 (Moon et al. 2020).

The shape model and spin state are the most fundamental parameters for predicting the evolutionary process due to Earth's tidal effect. In addition, these properties provide important information for planning space mission scenarios. The spin state and convex shape model of Apophis were reconstructed by Pravec et al. (2014) using photometric data obtained from the 2012−2013 apparition. They found it has non-principal axis rotation in a short-axis mode (SAM), with rotation and precession periods of 263 and 27.38 h, respectively, and an orientation of angular momentum vector of $\lambda_L = 250°$ and $\beta_L = -75°$. In addition, the convex shape model of Pravec et al. (2014) can be approximated by a prolate ellipsoid with a ratio of the greatest to intermediate principal moments of inertia (I_b/I_c) of 0.965 and a ratio of the greatest to smallest principal moment of inertia (I_a/I_c) of 0.61.

**Table 1.** Details of the observatories and instruments used in this campaign.

Telescope	Latitude	Longitude	Instrument
–Ground-based telescopes–			
ADYU60	37:45:06 N	38:13:32 E	Andor Tech
AMU Winer, RBT 0.7 m	31:39:56 N	110:36:06 W	Andor iXon
ATLAS HKO 0.5 m	20:42:27 N	156:15:25 W	STA-1600 10.5K CCD
ATLAS MLO 0.5 m	19:32:10 N	155:34:34 W	STA-1600 10.5K CCD
BOAO 1.8 m	36:09:53 N	128:58:36 E	E2V 4K CCD
CAHA 1.23 m	37:13:25 N	2:32:46 W	DLR MKIII camera
CAHA 2.2 m	37:13:25 N	2:32:46 W	CAFOS
DOAO 1.0 m	34:31:35 N	127:26:48 E	PI SOPHIA-2048B CCD
Kawabe Cosmic Park 1.0 m	33:53:27 N	135:13:12 E	FLI PL09000
KMTNet CTIO 1.6 m	30:10:02 S	70:48:14 W	18K mosaic CCD with four E2V 9K
KMTNet SAAO 1.6 m	32:22:43 S	20:48:37 E	18K mosaic CCD with four E2V 9K
KMTNet SSO 1.6 m	31:16:16 S	149:03:45 E	18K mosaic CCD with four E2V 9K
Krakow-CDK500 0.5 m	50:03:15 N	19:49:41 E	Apogee USB/Net
LCO CTIO A 1.0 m	30:10:03 S	70:48:17 W	Sinistro
LCO CTIO B 1.0 m	30:10:03 S	70:48:17 W	Sinistro
LCO McDonald A 1.0 m	30:41:47 S	104:00:54 E	Sinistro
LCO McDonald B 1.0 m	30:41:48 S	104:00:54 E	Sinistro
LCO SAAO A 1.0 m	32:23:50 N	20:48:37 W	Sinistro
LCO SAAO B 1.0 m	32:23:50 N	20:48:36 W	Sinistro
LCO SAAO C 1.0 m	32:23:51 N	20:48:36 W	Sinistro
LCO SSO A 1.0 m	31:16:22 N	149:04:14 W	Sinistro
LCO SSO B 1.0 m	31:16:23 N	149:04:15 W	Sinistro
LOAO 1.0 m	32:26:32 N	110:47:19 E	E2V 4K CCD
OWL Mitzpeh Ramon 0.5 m	30:35:51 N	34:45:48 E	FLI 16803
OWL Oukaimeden 0.5 m	31:12:21 N	7:52:00 W	FLI 16803
OWL Tucson 0.5 m	32:26:31 N	110:47:21 W	FLI 16803
OWL Yeongcheon 0.5 m	36:09:50 N	128:58:33 E	FLI 16803
SAAO Lesedi 1.0 m	32:22:47 S	20:48:36 E	SHOC (Andor iXon 888)
Skynet DSO-14, 0.4 m	36:15:01 N	81:24:45 W	Apogee USB/Net
Skynet Prompt5, 0.4 m	30:10:03 S	70:48:19 W	Apogee USB/Net
Skynet Prompt6, 0.4 m	30:10:03 S	70:48:19 W	FLI
Skynet Prompt MO 1 0.4 m	31:38:18 S	116:59:19 E	Apogee USB/Net
Skynet RRRT 0.6 m	37:52:44 N	78:41:39 W	SBIG STX-16803 3 CCD
SOAO 0.6 m	36:56:04 N	128:27:27 E	FLI 4K
Suhora Observatory Zeiss-60	49:34:09 N	20:04:03 E	Apogee AltaU-47
TUG 1.0 m	36:49:27 N	30:20:08 E	SI 4K
–Space-based telescope–			
TESS 0.1 m			Four MIT Lincoln Lab. CCID-80 devices

Notes. ADYU = Adiyaman University Astrophysics Application and Research Center, AMU = Adam Mickiewicz University, RBT = Roman Baranowski Telescope, ATLAS = Asteroid Terrestrial-impact Last Alert System, HKO = Haleakala Observatory, MLO = Mauna Loa Observatory, BOAO = Bohyunsan Optical Astronomy Observatory, DOAO = Deokheung Optical Astronomy Observatory, CAHA = Calar Alto Observatory, KMTNet = Korea Microlensing Telescope (Kim et al. 2016), CTIO = Cerro Tololo Inter-American Observatory, SAAO = South African Astronomical Observatory, SSO = Siding Spring Observatory, LCO = Las Cumbres Observatory, LOAO = Lemonsan Optical Astronomy Observatory, CDK = Corrected Dall-Kirkham, OWL = Optical Wide-field patroL Network, DSO = Dark Sky Observatory, MO = Meckering Observatory, RRRT = Rapid Response Robotic Telescope, SOAO = Sobaeksan Optical Astronomy Observatory, TUG = TÜBÍTAK National observatory, TESS = Transiting Exoplanet Survey Satellite, CAFOS = Calar Alto Faint Object Spectrograph.

For the last time before the 2029 Earth encounter, Apophis approached Earth on March 2021 at 0.11 AU and its apparent brightness increased to reach magnitude 16. Thus, the observation window for Apophis from the end of 2020 to the beginning of 2021 was the last opportunity to investigate its spin properties and refine the convex shape model. Therefore, we planned a photometric observation campaign for Apophis during this apparition. The details of our observation campaign are described in Sect. 2. In Sect. 3, a period analysis and reconstruction of the spin state and shape model of Apophis are reported. Finally, the summary and conclusions of this Letter are given in Sect. 4.

2. Photometric observation campaign during the 2020–2021 apparition

As mentioned above, the 2020−2021 apparition of Apophis was the last opportunity to study the physical properties of this asteroid before its 2029 close approach. Therefore, we organized an extensive and long-term photometric observation campaign for Apophis during this apparition. Our observation campaign was conducted using both the ground-based telescopes and the Transiting Exoplanet Survey Satellite (TESS) space telescope (Ricker et al. 2015). The details of the telescopes and instruments used in our campaign are provided in Table 1. The geometries
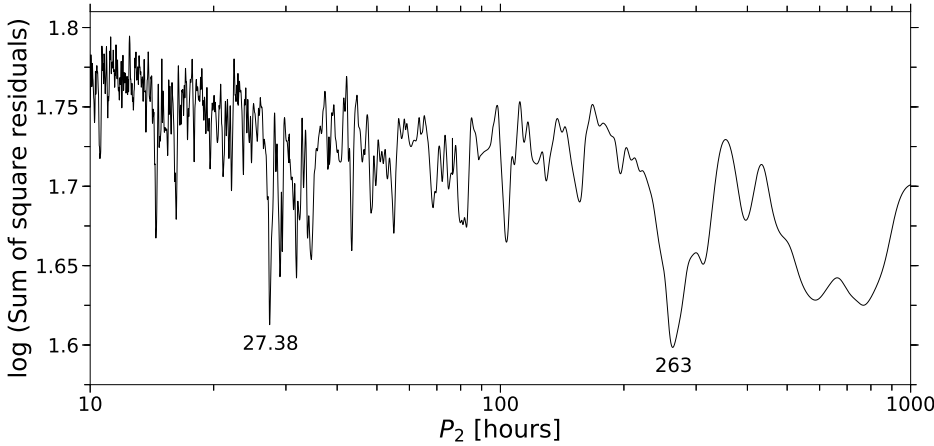
Fig. 1. P_2 search diagram of Apophis. The sum of square residuals was calculated for the fourth-order two-period Fourier series with $P_1 = 30.56\,$h fitted to our dense light curve obtained from February 7.0, 2021, to March 16.2, 2021 in flux units.

and observational circumstances are listed in Table A.1. This campaign's data also contributed to the global Apophis Planetary Defense Campaign (Reddy et al. 2022).

Ground-based observations were carried out in 11 countries, including the Republic of Korea, the US, Chile, South Africa, Australia, Poland, Spain, Turkey, and Japan using 36 telescopes. Through our observation campaign, we observed 214 dense-in-time light curves and two sparse-in-time light curves. The dense-in-time light curves were obtained using a Johnson-Cousins V or R filter except for the data from the Kawabe Cosmic Park, which used the Sloan Digital Sky Survey r' filter. All data reductions were conducted following standard procedures. However as the observations were made with different telescopes and instruments, the data reduction processes may differ slightly. The bias- and flat-field images were corrected, and the instrument magnitudes for each frame were measured using aperture photometry. All photometric data were calibrated with the ATLAS All-Sky Stellar Reference Catalog (ATLAS Refcat2; Tonry et al. 2018a). The ATLAS Refcat2 magnitudes were converted to Johnson–Cousins V and R magnitudes using empirical transformation equations (Tonry et al. 2012). The sparse-in-time light curves were obtained from ATLAS (Tonry et al. 2018a,b). The ATLAS light curve was observed between November 2020 and April 2021 using orange (o, 560−820 nm) and cyan (c, 420−650 nm) filters.

We also gathered long-term continuous photometric data observed from the TESS spacecraft using a wide I passband (see Fig. 1 in Ricker et al. 2015). TESS photometric data were obtained in a similar manner as done in Pál et al. (2020) for the image series of Sector 35 acquired between February 19, 2021, and March 7, 2021. The individual photometric data points were derived using a convolution-based differential image analysis by employing the tools of the FITSH package (Pál 2012).

3. Results

3.1. Periodic analysis

Before the shape model and spin state of Apophis were reconstructed, we performed periodic analysis of the light curve obtained from our observation campaign. To minimize the possible systematic effects caused by changes in the observing geometry, this analysis was only conducted using the dense-in-time light curves observed with phase angles from 20° to 40°, which corresponds to the period from February 7.0, 2021, to March 16.2, 2021. Because our observations were made with different filters, we corrected them to match the R filter using the color

indices $V - R = 0.38$, $R - T = 0.07$, and $r' - R = 0.33$. The data were converted to flux units, the heliocentric and geocentric distances were corrected to the unit distance, and the solar phase angle was converted to a consistent value using the $H - G$ phase relation and assuming $G = 0.24$. As Apophis exhibited tumbling motion, we attempted to detect double periods from the asteroid's light curve.

First, the Lomb-Scargle method (Lomb 1976; Scargle 1982) was adopted to search for periodicities in the light curve. The strongest signal in the Lomb-Scargle periodogram was found at a period of 15.28 h. In accordance with this method, we carried out a periodic analysis based on a single-peak light curve. However, most asteroid light curves have double peaks because their shapes are elongated. Therefore, we determined the primary period (P_1) on the light curve of Apophis to be 30.56 h, which is double the strongest signal in the Lomb-Scargle periodogram.

The secondary period (P_2) was determined using the two-period Fourier series method (Pravec et al. 2005, 2014). The two-period Fourier series employed in this analysis are presented as follows:

$$F(t) = C_0 + \sum_{j=1}^{m} \left[C_{j0} \cos \frac{2\pi j}{P_1} t + S_{j0} \sin \frac{2\pi j}{P_1} t \right]$$
$$+ \sum_{k=1}^{m} \sum_{j=-m}^{m} \left[C_{jk} \cos \left(\frac{2\pi j}{P_1} + \frac{2\pi k}{P_2} \right) t + S_{jk} \sin \left(\frac{2\pi j}{P_1} + \frac{2\pi k}{P_2} \right) t \right].$$

The result for the P_2 search is shown in Fig. 1, where the abscissa is P_2 and the ordinate is the sum of the squared residuals for the fitted fourth-order two-period Fourier series with $P_1 = 30.56\,$h. From our P_2 search, we found two minimums, at 27.38 and 263 h. As the long period of 263 h was a combination of the short period of 27.38 h with P_1, that is, $263^{-1} \approx 27.38^{-1} - 30.56^{-1}$, it seems to be derived from the short period. Thus, we determined P_2 to be 27.38 h. Figure 2 shows a composite light curve of Apophis obtained from February 7.0, 2021, to March 16.2, 2021 with the fitted fourth-order two-period Fourier series for periods of 30.56 and 27.38 h.

3.2. Reconstruction of the convex shape model and spin state from light curves

Given that the radar observation of Apophis suggests that it has a bifurcated shape (Brozović et al. 2018), the non-convex shape model may be a more suitable description of its actual shape.
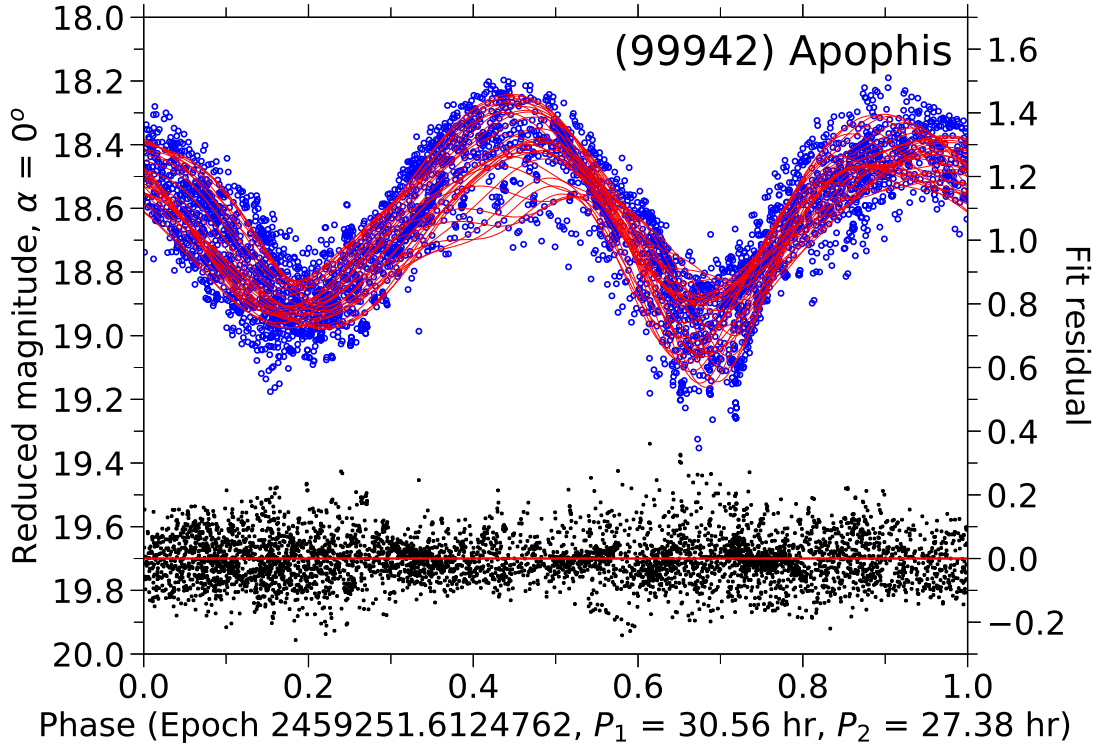
Fig. 2. Light curve of Apophis taken from February 7.0, 2021, to March 16.2, 2021 reduced to the unit geocentric and heliocentric distance and to a consistent solar phase angle. The blue open circles indicate the photometric data folded with P_1. The red curves denote the best-fit fourth-order two-period Fourier series with the periods $P_1 = 30.56$ h and $P_2 = 27.38$ h. The black squares indicate the residuals of the photometric data from the fourth-order two-period Fourier series (see the right ordinates).
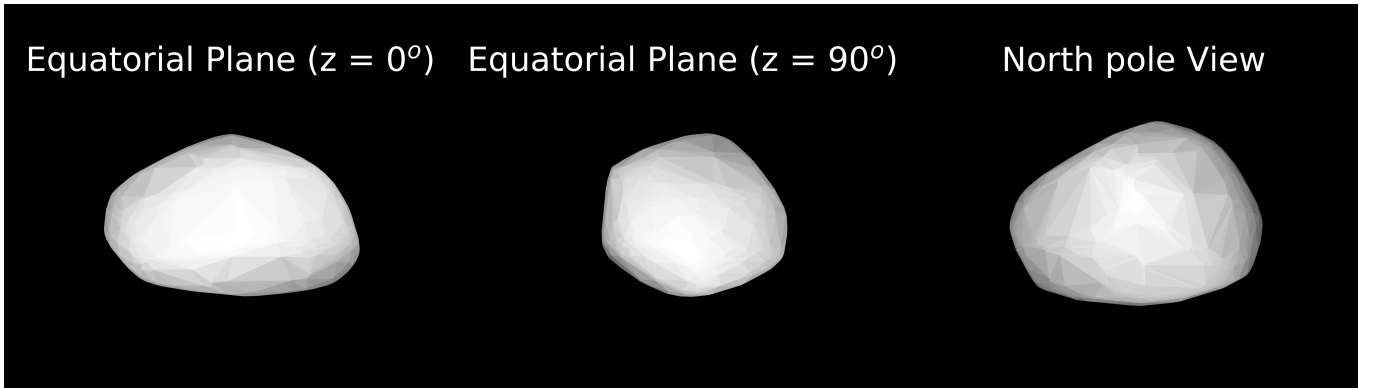
Fig. 3. Convex shape model of Apophis.

Nonetheless, this non-convex model obtained using photometric data should be applied only after very careful consideration. It is generally not possible to uniquely reconstruct a non-convex model using only photometric data (Viikinkoski et al. 2017; Harris & Warner 2020). Further, concavities can be revealed only when reconstruction is performed using data observed at sufficiently high phase angles (Ďurech & Kaasalainen 2003). Unfortunately, we did not obtain the data at the phase angles needed to create a non-convex model of Apophis. Therefore, our analysis was conducted based on the convex shape model.

The convex shape model and spin state of Apophis were reconstructed using the light-curve inversion method for the non-principal axis rotator (Kaasalainen & Torppa 2001; Kaasalainen et al. 2001; Kaasalainen 2001) combined with Hapke's light-scattering model (Hapke 1993). In this work, we used both the light curves obtained through our campaign obser-

vation and all available observation data collected from the literature. The historical light curves are listed in Table A.2.

The first step in revealing the spin state of a tumbling asteroid is to determine the physical periods, that is, the rotation (P_ψ) and precession period (P_ϕ). Because the periods on the light curve were derived from the physical periods, P_1^{-1} and P_2^{-1} usually appear at P_ϕ^{-1} and $P_\phi^{-1} \pm P_\psi^{-1}$, where the plus sign is for the long-axis mode (LAM) and the minus sign for the SAM (Kaasalainen 2001). Therefore, we found two possible physical period combinations using the periods obtained in the previous section: $P_1^{-1} = P_\phi^{-1}$ and $P_2^{-1} = P_\phi^{-1} + P_\psi^{-1}$ (LAM); $P_1^{-1} = P_\phi^{-1} - P_\psi^{-1}$ and $P_2^{-1} = P_\phi^{-1}$ (SAM). The optimization for each P_ϕ was performed in the same way as in Lee et al. (2020, 2021). In these procedure, the Hapke's model parameters were set to those of a typical S-type asteroid: $\varpi = 0.23$, $g = -0.27$, $h = 0.08$, $B_0 = 1.6$,

Table 2. Parameters of the Apophis model.

	This work	Pravec et al. (2014)
λ_L [deg]	278^{+9}_{-8}	250 ± 27
β_L [deg]	-86^{+5}_{-4}	-75 ± 14
P_ψ [h]	264.18 ± 0.03	263 ± 6
P_ϕ [h]	27.3855 ± 0.0003	27.38 ± 0.07
ψ_0 [a] [deg]	3^{+5}_{-1}	14^{+44}_{-11}
ϕ_0 [a] [deg]	183^{+7}_{-4}	152^{+173}_{-64}
I_a/I_c	$0.64^{+0.02}_{-0.09}$	$0.61^{+0.11}_{-0.08}$
I_b/I_c	$0.962^{+0.023}_{-0.002}$	$0.965^{+0.009}_{-0.015}$
$a_{\rm dyn}/c_{\rm dyn}$	1.48 ± 0.19	1.51 ± 0.18
$b_{\rm dyn}/c_{\rm dyn}$	1.06 ± 0.04	1.06 ± 0.02
$a_{\rm shape}/c_{\rm shape}$	1.56 ± 0.04	1.64 ± 0.09
$b_{\rm shape}/c_{\rm shape}$	1.12 ± 0.03	$1.14^{+0.04}_{-0.08}$
E/E_0	1.018 ± 0.010	1.024 ± 0.013

Notes. λ_L and β_L are the ecliptic coordinates of the constant angular momentum vector $\boldsymbol{L}$; ψ_0 and ϕ_0 are the standard Euler angles at epoch JD_0; I_a, I_b and I_c are the dynamical moments of inertia corresponding to the longest-, intermediate-, and shortest-axes; $a_{\rm dyn}/c_{\rm dyn}$ and $c_{\rm dyn}/c_{\rm dyn}$ are the axial ratios of a dynamically equivalent ellipsoid; $a_{\rm shape}/c_{\rm shape}$ and $c_{\rm shape}/c_{\rm shape}$ are the axial ratios of a convex shape model; E/E_0 is the ratio of the rotational kinetic energy to the lowest energy for the given angular momentum. [a]The epoch JD_0 is 2456284.676388 (December, 23.176388, 2012).

and $\bar{\theta} = 20°$ (Li et al. 2015). Because we did not obtain data observed at low solar phase angles, the parameters for the opposition surge, h and B_0, and the roughness, $\bar{\theta}$, were fixed. Only the ϖ and g parameters were optimized. It was found that the inertia tensor of the convex shape model for the LAM solution was not consistent with the kinematic I_1 and I_2 parameters. Therefore, we decided to use the SAM as the final solution.

The best-fit model for Apophis is listed in Table 2, together with the Pravec et al. (2014) solution for comparison. The uncertainties of our model parameters correspond to a 3σ confidence interval. The confidence interval was estimated from the increase in the χ^2 value when the solved-for physical parameters were varied. The threshold corresponding to the 3σ confidence interval was set as $\chi^2_{\rm min} \times (1 + 3\sqrt{2/\nu})^1$, where $\chi^2_{\rm min}$ represents the χ^2 value for the best-fit solution and ν represents the number of degrees of freedom (Vokrouhlický et al. 2017). The convex shape model of Apophis is shown in Fig. 3. The synthetic light curve of our model and the observed light curve are presented in Appendix B.

4. Summary and conclusions

In this Letter, we present the convex shape model and spin state of Apophis reconstructed using historical and newly obtained light curves. The new photometric data were observed from an extensive and long-term photometric observation campaign for Apophis during its 2020−2021 apparition using 36 facilities, including ground-based telescopes and TESS. We obtained 211 dense-in-time light curves and two spare-in-time light curves. In the period analysis conducted with our dense light curves, double periods of 30.56 and 27.38 h, respectively, were detected.

The best-fit solution indicates that Apophis is in a SAM state with rotation and precession periods of 264.178 ± 0.01

---

[1] These was a typo in Vokrouhlický et al. (2017), so we used $2/\nu$ instead of 2ν.

and 27.38547 ± 0.00002 h, respectively. The ecliptic coordinates of the angular momentum vector orientation of this asteroid are $(275 \pm 3°, -85 \pm 1°)$. In addition, the ratios of the dynamical moments of inertia were estimated to be $I_a/I_c = 0.64$ and $I_b/I_c = 0.96$. Our model is similar to that of Pravec et al. (2014). Nonetheless, the uncertainties of the model parameters were improved because they were reconstructed based on the data set obtained from the two apparitions. This model will be useful both for investigating changes in Apophis's physical properties due to the tidal effect during its encounter in 2029 and for planning a space mission to this asteroid.

References

Binzel, R. P., Rivkin, A. S., Thomas, C. A., et al. 2009, Icarus, 200, 480
Brozović, M., Benner, L. A. M., McMichael, J. G., et al. 2018, Icarus, 300, 115
Chesley, S. R. 2006, in Asteroids, Comets, Meteors, eds. D. Lazzaro, S. Ferraz-Mello, & J. A. Fernández, 229, 215
DeMartini, J. V., Richardson, D. C., Barnouin, O. S., et al. 2019, Icarus, 328, 93
Ďurech, J., & Kaasalainen, M. 2003, A&A, 404, 709
Giorgini, J. D., Benner, L. A. M., Ostro, S. J., Nolan, M. C., & Busch, M. W. 2008, Icarus, 193, 1
Greicius, T. 2021, NASA Analysis: Earth Is Safe From Asteroid Apophis for 100-Plus Years, accessed: 26-Mar-2021
Hapke, B. 1993, Theory of Reflectance and Emittance Spectroscopy (Cambridge: Cambridge University Press)
Harris, A., & Warner, B. D. 2020, Icarus, 339, 113602
Hirabayashi, M., Kim, Y., & Brozović, M. 2021, Icarus, 365, 114493
Kaasalainen, M. 2001, A&A, 376, 302
Kaasalainen, M., & Torppa, J. 2001, Icarus, 153, 24
Kaasalainen, M., Torppa, J., & Muinonen, K. 2001, Icarus, 153, 37
Kim, S.-L., Lee, C.-U., Park, B.-G., et al. 2016, J. Korean Astron. Soc., 49, 37
Lee, H. J., Ďurech, J., Kim, M. J., et al. 2020, A&A, 635, A137
Lee, H.-J., Ďurech, J., Vokrouhlický, D., et al. 2021, AJ, 161, 112
Li, J. Y., Helfenstein, P., Buratti, B., Takir, D., & Clark, B. E. 2015, in Asteroids IV, eds. P. Michel, F. E. DeMeo, & W. F. Bottke (Tucson: University of Arizona Press), 129
Lomb, N. R. 1976, Ap&SS, 39, 447
Moon, H. K., Choi, Y. J., Kim, M. J., et al. 2020, LPI Contrib., 2242, 2065
Pál, A. 2012, MNRAS, 421, 1825
Pál, A., Szakáts, R., Kiss, C., et al. 2020, ApJS, 247, 26
Pravec, P., Harris, A. W., Scheirich, P., et al. 2005, Icarus, 173, 108
Pravec, P., Scheirich, P., Ďurech, J., et al. 2014, Icarus, 233, 48
Reddy, V., Sanchez, J. A., Furfaro, R., et al. 2018, AJ, 155, 140

Reddy, V., Kelley, M. S., Dotson, J., et al. 2022, Planet. Sci. J., submitted
Ricker, G. R., Winn, J. N., Vanderspek, R., et al. 2015, J. Astron. Telesc. Instrum. Syst., 1, 014003
Scargle, J. D. 1982, ApJ, 263, 835
Souchay, J., Souami, D., Lhotka, C., Puente, V., & Folgueira, M. 2014, A&A, 563, A24
Souchay, J., Lhotka, C., Heron, G., et al. 2018, A&A, 617, A74
Tonry, J. L., Stubbs, C. W., Lykke, K. R., et al. 2012, ApJ, 750, 99
Tonry, J. L., Denneau, L., Flewelling, H., et al. 2018a, ApJ, 867, 105
Tonry, J. L., Denneau, L., Heinze, A. N., et al. 2018b, PASP, 130, 064505
Valvano, G., Winter, O. C., Sfair, R., et al. 2022, MNRAS, 510, 95
Viikinkoski, M., Hanuš, J., Kaasalainen, M., Marchis, F., & Ďurech, J. 2017, A&A, 607, A117
Vokrouhlický, D., Pravec, P., Ďurech, J., et al. 2017, AJ, 153, 270
Warner, B. D., & Stephens, R. D. 2021, Minor Planet Bull., 48, 294
Yu, Y., Richardson, D. C., Michel, P., Schwartz, S. R., & Ballouz, R.-L. 2014, Icarus, 242, 82

[1] Korea Astronomy and Space Science Institute, 776, Daedeokdae-ro, Yuseong-gu, Daejeon 34055, Korea
e-mail: hjlee@kasi.re.kr

[2] Astronomical Observatory Institute, Faculty of Physics, A. Mickiewicz University, Słoneczna 36, 60-286 Poznań, Poland

[3] Chungbuk National University, 1 Chungdae-ro, Seowon-gu, Cheongju, Chungbuk 28644, Korea

[4] University of Science and Technology, 217, Gajeong-ro, Yuseong-gu, Daejeon 34113, Korea

[5] Astronomical Observatory, Jagiellonian University, ul. Orla 171, 30-244 Kraków, Poland

[6] Mt. Suhora Observatory, Pedagogical University, ul. Pochorążych 2, 30-084 Kraków, Poland

[7] Las Cumbres Observatory, 6740 Cortona Drive Suite 102, Goleta, CA 93117, USA

[8] Las Cumbres Observatory, School of Physics and Astronomy, Cardiff University, Queens Buildings, The Parade, Cardiff CF24 3AA, UK

[9] Asteroid Institute, 20 Sunnyside Ave, Suite 427, Mill Valley, CA 94941, USA

[10] Department of Astronomy and the DIRAC Institute, University of Washington, 3910 15th Ave NE, Seattle, WA 98195, USA

[11] Konkoly Observatory, Research Centre for Astronomy and Earth Sciences, Eőtvős Loránd Research Network (ELKH), Konkoly Thege Miklós út 15-17, 1121 Budapest, Hungary

[12] South African Astronomical Observatory, Cape Town 7925, South Africa

[13] Department of Astronomy, University of Cape Town, Rondebosch 7701, South Africa

[14] Kepler Institute of Astronomy, University of Zielona Góra, Lubuska 2, 65-265 Zielona Góra, Poland

[15] Departamento de Sistema Solar, Instituto de Astrofísica de Andalucía (CSIC), Glorieta de la Astronomía s/n, 18008 Granada, Spain

[16] National Youth Space Center, Goheung, Jeollanam-do 59567, Korea

[17] Deutsches Zentrum für Luft- und Raumfahrt (DLR), Institute of Planetary Research, 12489 Berlin, Germany

[18] University of Occupational and Environmental Health, Japan, 1-1 Iseigaoka, Yahata, Kitakyusyu 807-8555, Japan

[19] Planetary Exploration Research Center, Chiba Institute of Technology, 2-17-1 Tsudanuma, Narashino, Chiba 275-0016, Japan

[20] University of North Carolina at Chapel Hill, Chapel Hill, NC 27599, USA

[21] Department of Physics, Adiyaman University, 02040 Adiyaman, Turkey

[22] Dark Sky Observatory, Dept. of Physics and Astronomy, Appalachian State University, Boone, NC 28608, USA

[23] Akdeniz University, Department of Space Sciences and Technologies, 07058 Antalya, Turkey

[24] TÜBİTAK National Observatory, Akdeniz University Campus, 07058 Antalya, Turkey

[25] Astrophysics Application and Research Center, Adiyaman University, Adiyaman 02040, Turkey

Appendix A: Additional tables

Table A.1. Geometries and observational circumstances.

Date UT	RA (h m)	Dec (° ′)	r_h (AU)	Δ (AU)	α (°)	Observatory	Filter
				–Dense photometry–			
2021-01-16.5	11 44	-17 26	1.076	0.203	58.2	LOAO	*R*
2021-01-17.5	11 43	-17 37	1.077	0.200	57.5	LOAO	*R*
2021-01-18.5	11 43	-17 48	1.078	0.198	56.7	LOAO	*R*
2021-01-29.1	11 34	-19 16	1.091	0.170	48.1	SAAO Lesedi	*VR*
2021-02-05.0	11 21	-19 33	1.096	0.153	41.4	SAAO Lesedi	*V*
2021-02-05.4	11 20	-19 33	1.096	0.152	41.0	Skynet Prompt5	*R*
2021-02-06.0	11 19	-19 31	1.096	0.151	40.3	SAAO Lesedi	*V*
2021-02-06.3	11 18	-19 31	1.096	0.150	40.0	OWL USA	*R*
2021-02-07.0	11 16	-19 29	1.097	0.148	39.3	CAHA 2.2 m	*R*
2021-02-07.1	11 16	-19 28	1.097	0.148	39.2	LCO SAAO A	*R*
2021-02-07.1	11 16	-19 28	1.097	0.148	39.2	LCO SAAO B	*R*
2021-02-07.1	11 16	-19 28	1.097	0.148	39.2	SAAO Lesedi	*V*
2021-02-07.2	11 16	-19 28	1.097	0.148	39.1	LCO CTIO A	*R*
2021-02-07.3	11 15	-19 28	1.097	0.148	38.9	OWL USA	*R*
2021-02-07.3	11 15	-19 28	1.097	0.148	38.9	Skynet Prompt5	*R*
2021-02-07.8	11 14	-19 26	1.097	0.147	38.4	LCO SAAO C	*R*
2021-02-08.0	11 14	-19 25	1.097	0.146	38.2	LCO SAAO A	*R*
2021-02-08.0	11 14	-19 25	1.097	0.146	38.2	LCO SAAO B	*R*
2021-02-08.1	11 13	-19 24	1.097	0.146	38.1	SAAO Lesedi	*V*
2021-02-08.3	11 13	-19 23	1.097	0.145	37.8	LCO CTIO A	*R*
2021-02-08.3	11 13	-19 23	1.097	0.145	37.8	LCO McDonald A	*R*
2021-02-08.3	11 13	-19 23	1.097	0.145	37.8	OWL USA	*R*
2021-02-08.3	11 13	-19 23	1.097	0.145	37.8	Skynet Prompt5	*R*
2021-02-08.6	11 12	-19 22	1.097	0.145	37.5	LCO SSO B	*R*
2021-02-08.9	11 11	-19 20	1.098	0.144	37.2	LCO SAAO A	*R*
2021-02-09.1	11 10	-19 19	1.098	0.144	37.0	LCO SAAO B	*R*
2021-02-09.1	11 10	-19 19	1.098	0.144	37.0	SAAO Lesedi	*V*
2021-02-09.3	11 10	-19 17	1.098	0.143	36.7	LCO McDonald B	*R*
2021-02-09.3	11 10	-19 17	1.098	0.143	36.7	Skynet Prompt5	*R*
2021-02-09.4	11 10	-19 17	1.098	0.143	36.6	OWL USA	*R*
2021-02-09.6	11 09	-19 15	1.098	0.142	36.4	LCO SSO B	*R*
2021-02-09.9	11 08	-19 13	1.098	0.142	36.1	LCO SAAO C	*R*
2021-02-10.0	11 08	-19 12	1.098	0.142	35.9	LCO SAAO A	*R*
2021-02-10.1	11 07	-19 12	1.098	0.141	35.8	LCO SAAO B	*R*
2021-02-10.1	11 07	-19 12	1.098	0.141	35.8	OWL MAR	*R*
2021-02-10.1	11 07	-19 12	1.098	0.141	35.8	SAAO Lesedi	*V*
2021-02-10.2	11 07	-19 11	1.098	0.141	35.7	Skynet Prompt5	*R*
2021-02-10.3	11 07	-19 10	1.098	0.141	35.6	LCO CTIO B	*R*
2021-02-10.4	11 07	-19 09	1.098	0.141	35.5	LCO McDonald B	*R*
2021-02-10.5	11 06	-19 08	1.098	0.140	35.4	LCO SSO B	*R*
2021-02-11.0	11 05	-19 04	1.098	0.139	34.8	Adiyaman Observatory	*R*
2021-02-11.0	11 05	-19 04	1.098	0.139	34.8	LCO SAAO C	*R*
2021-02-11.0	11 05	-19 04	1.098	0.139	34.8	OWL ISR	*R*
2021-02-11.1	11 04	-19 03	1.098	0.139	34.7	OWL MAR	*R*
2021-02-11.2	11 04	-19 02	1.098	0.139	34.6	LCO CTIO A	*R*
2021-02-11.3	11 04	-19 01	1.098	0.139	34.5	LCO CTIO B	*R*
2021-02-11.3	11 04	-19 01	1.098	0.139	34.5	Skynet Prompt5	*R*
2021-02-11.4	11 03	-19 00	1.098	0.139	34.3	Winer Observatory RBT	*R*
2021-02-11.5	11 03	-18 59	1.098	0.138	34.2	LCO SSO A	*R*
2021-02-11.5	11 03	-18 59	1.098	0.138	34.2	OWL USA	*R*
2021-02-12.0	11 01	-18 54	1.099	0.137	33.7	Adiyaman Observatory	*R*
2021-02-12.2	11 01	-18 52	1.099	0.137	33.4	OWL MAR	*R*
2021-02-12.3	11 00	-18 51	1.099	0.137	33.3	Winer Observatory RBT	*R*
2021-02-12.4	11 00	-18 50	1.099	0.136	33.2	OWL USA	*R*
2021-02-12.7	10 59	-18 46	1.099	0.136	32.9	Skynet Prompt MO1	*R*

Table A.1. continued.

Date UT	RA (h m)	Dec (° ′)	r_h (AU)	Δ (AU)	α (°)	Observatory	Filter
2021-02-13.2	10 57	-18 40	1.099	0.135	32.3	Skynet Prompt5	R
2021-02-14.0	10 54	-18 29	1.099	0.133	31.4	Adiyaman Observatory	R
2021-02-15.1	10 50	-18 13	1.099	0.131	30.1	CAHA 2.2 m	R
2021-02-16.1	10 47	-17 55	1.099	0.129	29.0	OWL MAR	R
2021-02-16.4	10 45	-17 50	1.099	0.129	28.6	Skynet Prompt5	R
2021-02-16.6	10 45	-17 46	1.099	0.128	28.4	Skynet Prompt MO1	R
2021-02-16.9	10 43	-17 40	1.099	0.128	28.1	OWL MAR	R
2021-02-17.4	10 41	-17 30	1.099	0.127	27.5	Winer Observatory RBT	R
2021-02-17.7	10 40	-17 24	1.099	0.127	27.2	Skynet Prompt MO1	R
2021-02-18.4	10 37	-17 09	1.099	0.125	26.5	LOAO	R
2021-02-18.4	10 37	-17 09	1.099	0.125	26.5	Winer Observatory RBT	R
2021-02-18.7	10 36	-17 02	1.099	0.125	26.1	SOAO	R
2021-02-18.8	10 36	-16 60	1.099	0.125	26.0	Skynet Prompt MO1	R
2021-02-19.0	10 35	-16 55	1.099	0.125	25.8	Suhora Observatory	R
2021-02-19.3	10 34	-16 48	1.099	0.124	25.5	LOAO	R
2021-02-19.3	10 34	-16 48	1.099	0.124	25.5	Winer Observatory RBT	R
2021-02-19.6	10 32	-16 40	1.099	0.124	25.2	BOAO	R
2021-02-19.6	10 32	-16 40	1.099	0.124	25.2	OWL KOR	R
2021-02-19.6	10 32	-16 40	1.099	0.124	25.2	SOAO	R
2021-02-19.7	10 32	-16 38	1.099	0.123	25.2	Skynet Prompt MO1	R
2021-02-20.3	10 29	-16 23	1.099	0.123	24.6	LOAO	R
2021-02-20.5	10 28	-16 17	1.099	0.122	24.4	Skynet Prompt MO1	R
2021-02-20.6	10 28	-16 15	1.099	0.122	24.3	BOAO	R
2021-02-21.0	10 26	-16 04	1.099	0.122	24.0	Suhora Observatory	R
2021-02-21.4	10 25	-15 52	1.099	0.121	23.6	Winer Observatory RBT	R
2021-02-21.6	10 24	-15 47	1.099	0.121	23.5	BOAO	R
2021-02-21.8	10 23	-15 41	1.099	0.121	23.3	OWL ISR	R
2021-02-22.5	10 20	-15 20	1.099	0.120	22.8	Skynet Prompt MO1	R
2021-02-22.7	10 19	-15 14	1.098	0.119	22.6	BOAO	R
2021-02-22.7	10 19	-15 14	1.098	0.119	22.6	Skynet Prompt MO1	R
2021-02-23.1	10 17	-15 01	1.098	0.119	22.4	OWL USA	R
2021-02-24.2	10 12	-14 25	1.098	0.118	21.8	OWL USA	R
2021-02-25.0	10 08	-13 58	1.098	0.117	21.4	Suhora Observatory	R
2021-02-26.2	10 03	-13 14	1.097	0.116	21.1	OWL USA	R
2021-02-27.2	09 58	-12 36	1.097	0.115	21.1	OWL USA	R
2021-02-28.0	09 54	-12 04	1.096	0.115	21.2	CAHA 2.2 m	R
2021-02-28.0	09 54	-12 04	1.096	0.115	21.2	Skynet Prompt5	R
2021-03-01.2	09 49	-11 14	1.096	0.114	21.5	OWL USA	R
2021-03-01.9	09 45	-10 45	1.095	0.114	21.9	TUG	R
2021-03-03.0	09 40	-09 57	1.095	0.113	22.6	OWL MAR	R
2021-03-03.0	09 40	-09 57	1.095	0.113	22.6	Suhora Observatory	R
2021-03-03.0	09 40	-09 57	1.095	0.113	22.6	KMTNet CTIO	VR
2021-03-03.0	09 40	-09 57	1.095	0.113	22.6	Skynet Prompt5	R
2021-03-03.2	09 39	-09 48	1.095	0.113	22.7	OWL USA	R
2021-03-03.2	09 39	-09 48	1.095	0.113	22.7	Winer Observatory RBT	R
2021-03-03.4	09 39	-09 39	1.095	0.113	22.9	KMTNet SSO	VR
2021-03-05.1	09 31	-08 21	1.093	0.113	24.4	LCO CTIO A	R
2021-03-05.2	09 30	-08 16	1.093	0.113	24.5	LCO McDonald A	R
2021-03-05.4	09 30	-08 07	1.093	0.113	24.7	LCO SSO B	R
2021-03-05.6	09 29	-07 58	1.093	0.113	24.9	LCO SSO A	R
2021-03-05.8	09 28	-07 48	1.093	0.113	25.1	LCO SAAO A	R
2021-03-05.8	09 28	-07 48	1.093	0.113	25.1	LCO SAAO C	R
2021-03-06.4	09 25	-07 20	1.092	0.113	25.8	LCO SSO B	R
2021-03-06.5	09 25	-07 15	1.092	0.113	25.9	LCO SSO A	R
2021-03-06.8	09 23	-07 01	1.092	0.113	26.3	LCO SAAO C	R
2021-03-06.8	09 23	-07 01	1.092	0.113	26.3	OWL ISR	R
2021-03-06.9	09 23	-06 56	1.092	0.113	26.4	LCO SAAO A	R
2021-03-06.9	09 23	-06 56	1.092	0.113	26.4	OAUJ CDK500	R

Table A.1. continued.

Date UT	RA (h m)	Dec (° ′)	r_h (AU)	Δ (AU)	α (°)	Observatory	Filter
2021-03-07.0	09 22	-06 51	1.092	0.113	26.5	LCO CTIO B	R
2021-03-07.1	09 22	-06 47	1.092	0.113	26.6	OWL USA	R
2021-03-07.2	09 22	-06 42	1.092	0.113	26.8	LCO McDonald A	R
2021-03-07.3	09 21	-06 37	1.092	0.113	26.9	LCO McDonald B	R
2021-03-07.4	09 21	-06 32	1.092	0.113	27.0	KMTNet SSO	VR
2021-03-07.5	09 20	-06 27	1.091	0.113	27.1	LCO SSO A	R
2021-03-07.6	09 20	-06 23	1.091	0.113	27.3	LCO SSO B	R
2021-03-07.8	09 19	-06 13	1.091	0.113	27.5	KMTNet SAAO	VR
2021-03-07.8	09 19	-06 13	1.091	0.113	27.5	LCO SAAO A	R
2021-03-07.9	09 19	-06 08	1.091	0.113	27.6	LCO SAAO C	R
2021-03-08.0	09 18	-06 03	1.091	0.113	27.8	LCO CTIO B	R
2021-03-08.1	09 18	-05 58	1.091	0.113	27.9	LCO McDonald A	R
2021-03-08.2	09 17	-05 54	1.091	0.113	28.0	LCO McDonald B	R
2021-03-08.8	09 15	-05 25	1.090	0.113	28.8	OWL ISR	R
2021-03-08.9	09 14	-05 20	1.090	0.113	29.0	LCO SAAO C	R
2021-03-09.0	09 14	-05 15	1.090	0.113	29.1	LCO CTIO B	R
2021-03-09.0	09 14	-05 15	1.090	0.113	29.1	LCO SAAO B	R
2021-03-09.5	09 12	-04 51	1.090	0.113	29.8	LCO SSO A	R
2021-03-09.6	09 12	-04 46	1.090	0.113	29.9	LCO SSO B	R
2021-03-09.6	09 12	-04 46	1.090	0.113	29.9	SOAO	R
2021-03-09.8	09 11	-04 36	1.089	0.113	30.2	KMTNet SAAO	VR
2021-03-09.8	09 11	-04 36	1.089	0.113	30.2	LCO SAAO B	R
2021-03-10.0	09 10	-04 26	1.089	0.113	30.5	Suhora Observatory	R
2021-03-10.2	09 09	-04 16	1.089	0.114	30.8	LCO CTIO A	R
2021-03-10.2	09 09	-04 16	1.089	0.114	30.8	Skynet DSO-14	R
2021-03-10.3	09 09	-04 12	1.089	0.114	30.9	OWL USA	R
2021-03-10.3	09 09	-04 12	1.089	0.114	30.9	Skynet RRRT	R
2021-03-10.3	09 09	-04 12	1.089	0.114	30.9	Winer Observatory RBT	R
2021-03-10.5	09 08	-04 02	1.089	0.114	31.2	BOAO	R
2021-03-10.5	09 08	-04 02	1.089	0.114	31.2	DOAO	R
2021-03-10.6	09 08	-03 57	1.089	0.114	31.3	SOAO	R
2021-03-10.6	09 08	-03 57	1.089	0.114	31.3	Kawabe Observatory	r′
2021-03-10.9	09 06	-03 42	1.088	0.114	31.8	CAHA 1.23 m	R
2021-03-10.9	09 06	-03 42	1.088	0.114	31.8	OAUJ CDK500	R
2021-03-11.0	09 06	-03 37	1.088	0.114	31.9	Suhora Observatory	R
2021-03-11.1	09 06	-03 33	1.088	0.114	32.1	LCO CTIO B	R
2021-03-11.2	09 05	-03 28	1.088	0.114	32.2	Skynet RRRT	R
2021-03-11.3	09 05	-03 23	1.088	0.114	32.4	OWL USA	R
2021-03-11.3	09 05	-03 23	1.088	0.114	32.4	Winer Observatory RBT	R
2021-03-11.8	09 03	-02 59	1.087	0.114	33.1	LCO SAAO A	R
2021-03-11.9	09 02	-02 54	1.087	0.114	33.2	LCO SAAO B	R
2021-03-11.9	09 02	-02 54	1.087	0.114	33.2	LCO SAAO C	R
2021-03-12.0	09 02	-02 49	1.087	0.114	33.4	LCO CTIO B	R
2021-03-12.2	09 01	-02 39	1.087	0.115	33.7	LCO CTIO A	R
2021-03-12.3	09 01	-02 34	1.087	0.115	33.8	Winer Observatory RBT	R
2021-03-12.6	08 60	-02 20	1.086	0.115	34.3	LCO SSO A	R
2021-03-12.7	08 60	-02 15	1.086	0.115	34.4	LCO SAAO B	R
2021-03-12.9	08 59	-02 05	1.086	0.115	34.7	LCO SAAO A	R
2021-03-12.9	08 59	-02 05	1.086	0.115	34.7	OAUJ CDK500	R
2021-03-12.9	08 59	-02 05	1.086	0.115	34.7	Suhora Observatory	R
2021-03-13.2	08 58	-01 51	1.086	0.115	35.2	LCO CTIO B	R
2021-03-13.6	08 56	-01 36	1.086	0.115	35.6	DOAO	R
2021-03-13.8	08 56	-01 22	1.085	0.116	36.1	TUG	R
2021-03-13.9	08 55	-01 17	1.085	0.116	36.2	LCO SAAO A	R
2021-03-14.0	08 55	-01 12	1.085	0.116	36.4	Skynet Prompt5	R
2021-03-14.0	08 55	-01 12	1.085	0.116	36.4	Skynet RRRT	R
2021-03-14.1	08 54	-01 07	1.085	0.116	36.5	LCO CTIO B	R
2021-03-14.3	08 54	+00 58	1.085	0.116	36.8	LCO McDonald A	R

Table A.1. continued.

Date UT	RA (h m)	Dec (° ′)	r_h (AU)	Δ (AU)	α (°)	Observatory	Filter
2021-03-14.5	08 53	+00 48	1.084	0.116	37.1	BOAO	R
2021-03-15.0	08 51	+00 25	1.084	0.116	37.9	OAUJ CDK500	R
2021-03-15.0	08 51	+00 25	1.084	0.116	37.9	Skynet Prompt5	R
2021-03-15.1	08 51	+00 20	1.084	0.117	38.0	Skynet Prompt6	R
2021-03-15.1	08 51	+00 20	1.084	0.117	38.0	Skynet RRRT	R
2021-03-15.2	08 51	+00 15	1.084	0.117	38.2	LOAO	R
2021-03-15.9	08 48	+00 18	1.083	0.117	39.3	OAUJ CDK500	R
2021-03-16.0	08 48	+00 22	1.083	0.117	39.4	CAHA 2.2 m	R
2021-03-16.2	08 47	+00 32	1.082	0.118	39.7	LOAO	R
2021-03-16.6	08 46	+00 50	1.082	0.118	40.3	BOAO	R
2021-03-16.6	08 46	+00 50	1.082	0.118	40.3	DOAO	R
2021-03-16.9	08 45	+01 04	1.081	0.118	40.8	Adiyaman Observatory	R
2021-03-17.0	08 45	+01 09	1.081	0.118	40.9	CAHA 2.2 m	R
2021-03-17.0	08 45	+01 09	1.081	0.118	40.9	Skynet Prompt5	R
2021-03-17.1	08 45	+01 13	1.081	0.118	41.1	Skynet Prompt6	R
2021-03-17.6	08 43	+01 32	1.081	0.119	41.7	DOAO	R
2021-03-18.0	08 42	+01 55	1.080	0.119	42.4	CAHA 2.2 m	R
2021-03-18.2	08 41	+02 04	1.080	0.119	42.7	OWL USA	R
2021-03-18.4	08 41	+02 13	1.079	0.120	43.0	KMTNet SSO	VR
2021-03-18.8	08 40	+02 31	1.079	0.120	43.6	KMTNet SAAO	VR
2021-03-18.8	08 40	+02 31	1.079	0.120	43.6	OWL ISR	R
2021-03-19.2	08 38	+02 48	1.078	0.120	44.2	OWL USA	R
2021-03-19.9	08 37	+03 19	1.077	0.121	45.2	OWL ISR	R
2021-03-20.2	08 36	+03 32	1.077	0.122	45.7	OWL USA	R
2021-03-20.2	08 36	+03 32	1.077	0.122	45.7	Skynet RRRT	R
2021-03-21.2	08 33	+04 15	1.076	0.123	47.1	OWL USA	R
2021-03-22.3	08 30	+05 01	1.074	0.124	48.7	OWL USA	R
2021-03-22.5	08 30	+05 10	1.074	0.124	49.0	DOAO	R
2021-03-22.8	08 29	+05 22	1.073	0.125	49.4	KMTNet SAAO	VR
2021-03-24.8	08 25	+06 42	1.070	0.127	52.2	KMTNet SAAO	VR
2021-03-30.0	08 16	+09 53	1.061	0.134	59.0	KMTNet CTIO	VR
2021-03-30.7	08 15	+10 16	1.060	0.135	59.9	KMTNet SAAO	VR
2021-04-01.8	08 12	+11 25	1.055	0.138	62.5	KMTNet SAAO	VR
2021-04-03.1	08 11	+12 06	1.053	0.139	64.1	KMTNet CTIO	VR
2021-04-04.9	08 09	+13 00	1.049	0.142	66.2	CAHA 1.23 m	R
2021-04-05.4	08 08	+13 15	1.048	0.142	66.7	KMTNet SSO	VR
2021-04-05.9	08 08	+13 30	1.047	0.143	67.3	CAHA 1.23 m	R
2021-04-08.4	08 06	+14 39	1.042	0.146	70.1	KMTNet SSO	VR
2021-04-08.8	08 06	+14 50	1.041	0.147	70.6	KMTNet SAAO	VR
2021-04-14.8	08 02	+17 22	1.026	0.154	77.1	KMTNet SAAO	VR
2021-04-16.8	08 02	+18 09	1.021	0.156	79.2	KMTNet SAAO	VR
2021-04-18.4	08 01	+18 45	1.017	0.158	80.8	KMTNet SSO	VR
2021-04-18.8	08 01	+18 54	1.016	0.158	81.2	KMTNet SAAO	VR
2021-04-20.4	08 01	+19 29	1.012	0.160	82.9	KMTNet SSO	VR
–Sparse Photometry–							
2020-11-12 2021-04-09						ATLAS	c
2020-12-01 2021-04-03						ATLAS	o
–Space-based Photometry–							
2021-02-19 2021-03-07						TESS	wide I

Notes. RA: Right ascension, Dec: Declination, Δ: geocentric distance, r_h: heliocentric distance, α: phase angle.

Table A.2. List of the historical light curves.

Date UT	RA (h m)	Dec (° ′)	r_h (AU)	Δ (AU)	α (°)	References
2012-12-23.3	10 42	-27 22	1.000	0.102	77.6	Pravec et al. (2014)
2012-12-25.3	10 33	-27 23	1.006	0.101	74.3	Pravec et al. (2014)
2012-12-26.3	10 28	-27 23	1.009	0.101	72.7	Pravec et al. (2014)
2012-12-27.2	10 23	-27 21	1.011	0.101	71.2	Pravec et al. (2014)
2012-12-28.2	10 18	-27 19	1.014	0.100	69.5	Pravec et al. (2014)
2012-12-29.2	10 13	-27 14	1.017	0.100	67.8	Pravec et al. (2014)
2012-12-30.2	10 08	-27 10	1.019	0.099	66.2	Pravec et al. (2014)
2012-12-31.2	10 03	-27 03	1.022	0.099	64.5	Pravec et al. (2014)
2013-01-03.2	09 47	-26 34	1.029	0.098	59.5	Pravec et al. (2014)
2013-01-04.2	09 41	-26 20	1.032	0.097	57.9	Pravec et al. (2014)
2013-01-05.2	09 36	-26 06	1.034	0.097	56.2	Pravec et al. (2014)
2013-01-06.1	09 30	-25 51	1.036	0.097	54.7	Pravec et al. (2014)
2013-01-06.2	09 30	-25 49	1.036	0.097	54.6	Pravec et al. (2014)
2013-01-07.2	09 24	-25 30	1.039	0.097	52.9	Pravec et al. (2014)
2013-01-07.6	09 22	-25 22	1.040	0.097	52.3	Pravec et al. (2014)
2013-01-08.1	09 19	-25 11	1.041	0.097	51.5	Pravec et al. (2014)
2013-01-08.1	09 19	-25 11	1.041	0.097	51.5	Pravec et al. (2014)
2013-01-08.2	09 18	-25 10	1.041	0.097	51.3	Pravec et al. (2014)
2013-01-09.1	09 13	-24 49	1.043	0.097	49.9	Pravec et al. (2014)
2013-01-09.1	09 13	-24 49	1.043	0.097	49.9	Pravec et al. (2014)
2013-01-09.2	09 12	-24 46	1.043	0.097	49.7	Pravec et al. (2014)
2013-01-09.3	09 12	-24 44	1.043	0.097	49.5	Pravec et al. (2014)
2013-01-10.1	09 07	-24 24	1.045	0.097	48.3	Pravec et al. (2014)
2013-01-10.2	09 06	-24 22	1.045	0.097	48.1	Pravec et al. (2014)
2013-01-10.3	09 06	-24 19	1.046	0.097	48.0	Pravec et al. (2014)
2013-01-11.1	09 01	-23 57	1.047	0.097	46.7	Pravec et al. (2014)
2013-01-11.3	09 00	-23 52	1.048	0.097	46.4	Pravec et al. (2014)
2013-01-11.5	08 59	-23 46	1.048	0.097	46.1	Pravec et al. (2014)
2013-01-12.1	08 55	-23 28	1.049	0.097	45.2	Pravec et al. (2014)
2013-01-12.2	08 55	-23 25	1.050	0.097	45.1	Pravec et al. (2014)
2013-01-12.2	08 55	-23 25	1.050	0.097	45.1	Pravec et al. (2014)
2013-01-13.1	08 49	-22 57	1.051	0.097	43.7	Pravec et al. (2014)
2013-01-13.2	08 49	-22 54	1.052	0.097	43.6	Pravec et al. (2014)
2013-01-14.1	08 44	-22 24	1.053	0.097	42.3	Pravec et al. (2014)
2013-01-14.1	08 44	-22 24	1.053	0.097	42.3	Pravec et al. (2014)
2013-01-14.2	08 43	-22 20	1.054	0.097	42.2	Pravec et al. (2014)
2013-01-15.1	08 38	-21 49	1.055	0.098	40.9	Pravec et al. (2014)
2013-01-15.2	08 37	-21 45	1.056	0.098	40.8	Pravec et al. (2014)
2013-01-15.5	08 35	-21 34	1.056	0.098	40.4	Pravec et al. (2014)
2013-01-16.1	08 32	-21 12	1.057	0.098	39.6	Pravec et al. (2014)
2013-01-16.1	08 32	-21 12	1.057	0.098	39.6	Pravec et al. (2014)
2013-01-16.3	08 31	-21 04	1.058	0.098	39.4	Pravec et al. (2014)
2013-01-16.3	08 31	-21 04	1.058	0.098	39.4	Pravec et al. (2014)
2013-01-19.1	08 15	-19 11	1.063	0.100	36.2	Pravec et al. (2014)
2013-01-19.2	08 15	-19 07	1.063	0.100	36.1	Pravec et al. (2014)
2013-01-20.1	08 10	-18 28	1.065	0.101	35.2	Pravec et al. (2014)
2013-01-20.2	08 10	-18 24	1.065	0.101	35.1	Pravec et al. (2014)
2013-01-22.2	07 59	-16 54	1.068	0.103	33.5	Pravec et al. (2014)
2013-01-22.3	07 59	-16 50	1.068	0.103	33.5	Pravec et al. (2014)
2013-01-23.1	07 55	-16 13	1.070	0.104	33.0	Pravec et al. (2014)
2013-01-23.2	07 55	-16 08	1.070	0.104	32.9	Pravec et al. (2014)
2013-01-24.1	07 50	-15 26	1.071	0.105	32.4	Pravec et al. (2014)
2013-01-24.2	07 50	-15 22	1.071	0.105	32.4	Pravec et al. (2014)
2013-01-24.3	07 49	-15 17	1.072	0.105	32.4	Pravec et al. (2014)
2013-02-04.1	07 10	-06 46	1.086	0.123	33.8	Pravec et al. (2014)
2013-02-05.1	07 07	-06 01	1.087	0.125	34.4	Pravec et al. (2014)

Table A.2. continued.

Date UT	RA (h m)	Dec (° ′)	r_h (AU)	Δ (AU)	α (°)	References
2013-02-05.3	07 07	-05 53	1.087	0.126	34.5	Pravec et al. (2014)
2013-02-06.1	07 05	-05 17	1.088	0.128	35.0	Pravec et al. (2014)
2013-02-06.2	07 04	-05 13	1.088	0.128	35.1	Pravec et al. (2014)
2013-02-06.9	07 03	-04 43	1.089	0.129	35.5	Pravec et al. (2014)
2013-02-07.1	07 02	-04 34	1.089	0.130	35.7	Pravec et al. (2014)
2013-02-07.2	07 02	-04 29	1.089	0.130	35.7	Pravec et al. (2014)
2013-02-08.1	07 00	-03 51	1.090	0.132	36.4	Pravec et al. (2014)
2013-02-08.2	07 00	-03 47	1.090	0.132	36.4	Pravec et al. (2014)
2013-02-12.1	06 53	-01 09	1.093	0.142	39.3	Pravec et al. (2014)
2013-02-13.1	06 52	-00 31	1.094	0.145	40.1	Pravec et al. (2014)
2013-02-13.2	06 52	-00 27	1.094	0.145	40.2	Pravec et al. (2014)
2013-02-14.2	06 50	+00 10	1.094	0.148	40.9	Pravec et al. (2014)
2013-02-14.2	06 50	+00 10	1.094	0.148	40.9	Pravec et al. (2014)
2013-02-15.1	06 49	+00 43	1.095	0.150	41.6	Pravec et al. (2014)
2013-02-15.1	06 49	+00 43	1.095	0.150	41.6	Pravec et al. (2014)
2013-02-16.0	06 48	+01 15	1.095	0.152	42.3	Pravec et al. (2014)
2013-02-16.2	06 48	+01 22	1.096	0.153	42.5	Pravec et al. (2014)
2013-02-16.2	06 48	+01 22	1.096	0.153	42.5	Pravec et al. (2014)
2013-02-17.0	06 48	+01 49	1.096	0.155	43.0	Pravec et al. (2014)
2013-02-17.2	06 47	+01 56	1.096	0.156	43.2	Pravec et al. (2014)
2013-02-17.2	06 47	+01 56	1.096	0.156	43.2	Pravec et al. (2014)
2013-02-18.0	06 47	+02 23	1.096	0.158	43.8	Pravec et al. (2014)
2013-02-18.0	06 47	+02 23	1.096	0.158	43.8	Pravec et al. (2014)
2013-02-18.2	06 47	+02 30	1.096	0.159	44.0	Pravec et al. (2014)
2013-02-19.9	06 46	+03 25	1.097	0.163	45.2	Pravec et al. (2014)
2013-03-09.1	06 49	+10 38	1.096	0.215	56.3	Pravec et al. (2014)
2013-03-10.2	06 50	+11 00	1.095	0.218	56.9	Pravec et al. (2014)
2013-03-11.0	06 51	+11 15	1.095	0.221	57.3	Pravec et al. (2014)
2013-03-12.0	06 52	+11 33	1.094	0.224	57.9	Pravec et al. (2014)
2013-03-13.0	06 53	+11 51	1.094	0.227	58.4	Pravec et al. (2014)
2013-04-09.0	07 33	+17 20	1.060	0.297	70.7	Pravec et al. (2014)
2013-04-12.0	07 38	+17 43	1.054	0.303	71.9	Pravec et al. (2014)
2013-04-14.1	07 42	+17 57	1.050	0.307	72.8	Pravec et al. (2014)
2013-04-15.0	07 44	+18 03	1.048	0.308	73.2	Pravec et al. (2014)
2021-03-18.3	08 41	+02 08	1.080	0.120	42.9	Warner & Stephens (2021)
2021-03-19.2	08 38	+02 48	1.078	0.120	44.2	Warner & Stephens (2021)
2021-03-20.3	08 35	+03 37	1.077	0.122	45.8	Warner & Stephens (2021)
2021-03-21.2	08 33	+04 15	1.076	0.123	47.1	Warner & Stephens (2021)
2021-03-22.3	08 30	+05 01	1.074	0.124	48.7	Warner & Stephens (2021)
2021-03-23.3	08 28	+05 42	1.072	0.125	50.1	Warner & Stephens (2021)
2021-03-24.2	08 26	+06 19	1.071	0.126	51.4	Warner & Stephens (2021)
2021-03-27.2	08 20	+08 13	1.066	0.130	55.4	Warner & Stephens (2021)
2021-03-28.2	08 19	+08 50	1.064	0.131	56.7	Warner & Stephens (2021)
2021-03-29.2	08 17	+09 25	1.062	0.133	58.0	Warner & Stephens (2021)
2021-03-30.2	08 16	+09 59	1.060	0.134	59.3	Warner & Stephens (2021)
2021-03-31.2	08 14	+10 33	1.059	0.135	60.5	Warner & Stephens (2021)

Notes. RA: Right ascension, Dec: Declination, Δ: geocentric distance, r_h: heliocentric distance, α: phase angle.

Appendix B: Light curves
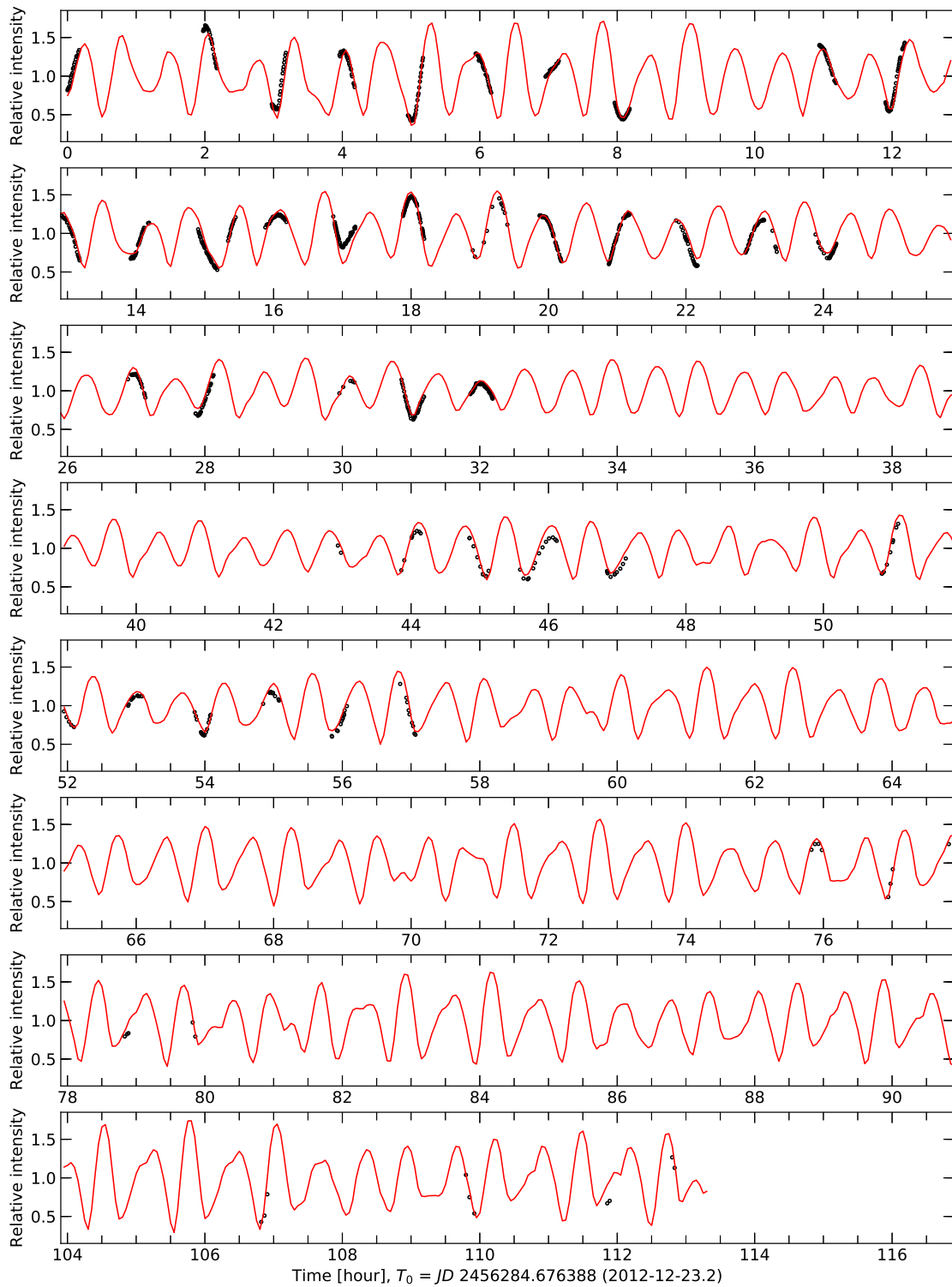
Fig. B.1. Photometric data from 2012-2013 (black open circle) with the synthetic light curve from the best-fit model (red line).
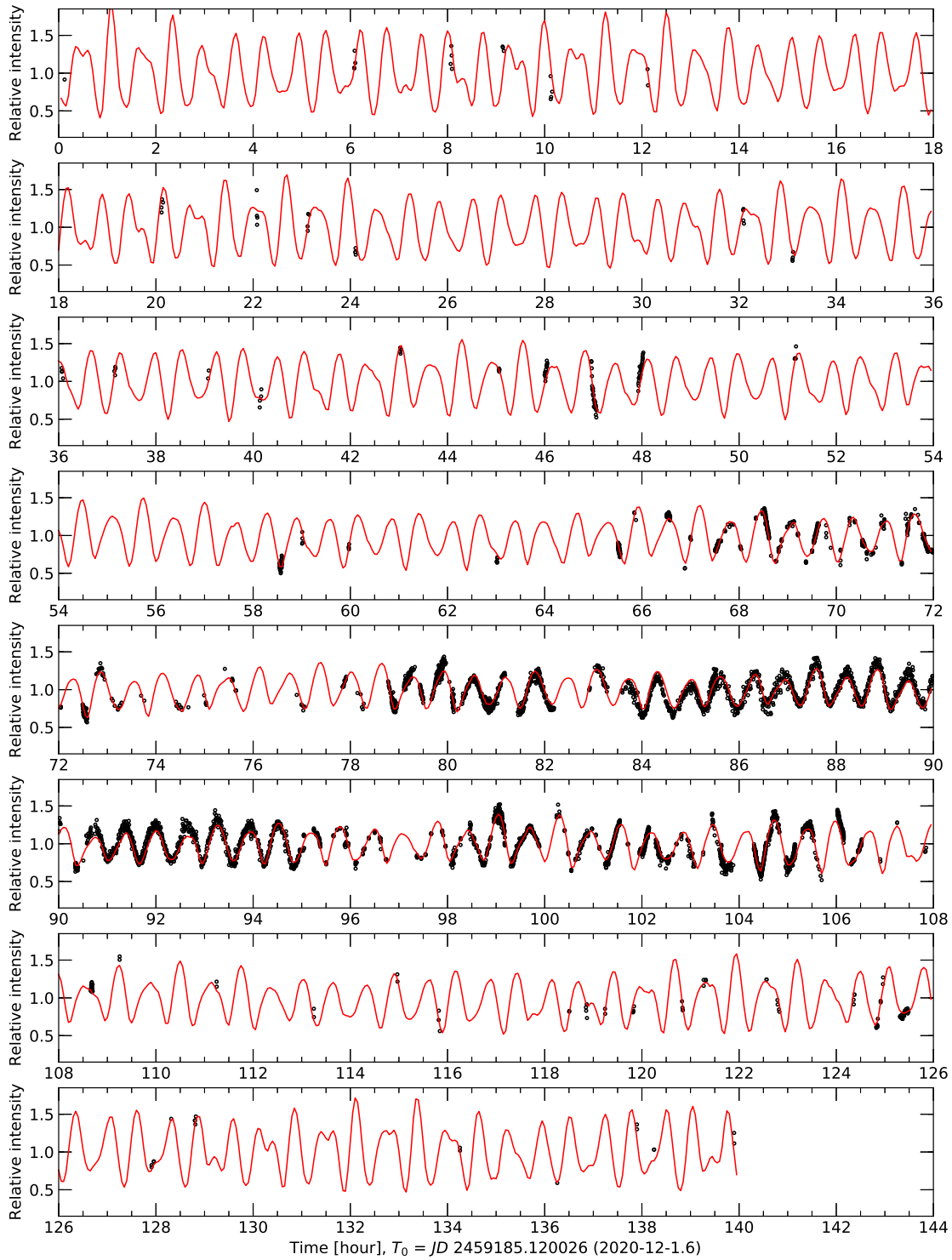
Fig. B.2. Photometric data from 2020-2021 (black open circle) with the synthetic light curve from the best-fit model (red line).